

# Probing the baryon mass fraction in IGM and its redshift evolution with fast radio bursts using Bayesian inference method

Hai-Nan Lin<sup>1,2</sup>, Rui Zou<sup>1,2\*</sup>

<sup>1</sup>*Department of Physics, Chongqing University, Chongqing 401331, China*

<sup>2</sup>*Chongqing Key Laboratory for Strongly Coupled Physics, Chongqing University, Chongqing 401331, China*

Accepted 2023; Received 2023; in original form 2023

## ABSTRACT

We investigate the fraction of baryon mass in intergalactic medium ( $f_{\text{IGM}}$ ), using 18 well-localized FRBs in the redshift range  $z \in (0.0039, 0.66)$ . We construct a five-parameter Bayesian inference model, with the probability distributions of dispersion measures (DM) of IGM and host galaxy properly taken into account. To check the possible redshift evolution, we parameterize  $f_{\text{IGM}}$  as a mildly evolving function of redshift,  $f_{\text{IGM}} = f_{\text{IGM},0}[1 + \alpha z/(1+z)]$ . By simultaneously constraining five parameters, we get  $f_{\text{IGM},0} = 0.92^{+0.06}_{-0.12}$  and  $\alpha = 0.49^{+0.59}_{-0.47}$ , and the median value of DM of host galaxy is  $\exp(\mu) = 72.49^{+33.31}_{-25.62}$  pc cm<sup>-3</sup>. By fixing two parameters which can be constrained independently with other observations, we obtain  $\alpha = 0.11^{+0.24}_{-0.27}$  in the three-parameter fit, which is consistent with zero within  $1\sigma$  uncertainty. Monte Carlo simulations show that even 300 FRBs are not enough to tightly constrain five parameters simultaneously. This is mainly caused by the correlation between parameters. Only if two parameters are fixed, 100 FRBs are necessary to achieve unbiased constraints on the remaining parameters.

**Key words:** fast radio bursts – intergalactic medium – cosmological parameters

## 1 INTRODUCTION

Fast radio bursts (FRBs) are millisecond-duration radio transients that randomly happen in the sky (Cordes & Chatterjee 2019; Petroff et al. 2019; Xiao et al. 2021; Zhang 2022). FRBs were first detected by the Parkes telescope in 2007 (Lorimer et al. 2007), and several hundred FRB sources have been collected till now (Petroff et al. 2016; Amiri et al. 2021). Among them only one is confirmed to originate from the Milky Way (Andersen et al. 2020; Bochenek et al. 2020), while the others are expected to have extragalactic origins (Keane et al. 2016; Chatterjee et al. 2017; Tendulkar et al. 2017). Generally, FRBs can be divided into two types, i.e., repeaters and non-repeaters, distinguished by whether they flash only once or more. But it is still unclear if the apparently non-repeaters will repeat or not in the future. Since the discovery of the first repeating event FRB 121102 with a redshift measurement of  $z = 0.19$  (Spitler et al. 2016; Scholz et al. 2016; Chatterjee et al. 2017; Marcote et al. 2017; Tendulkar et al. 2017), FRBs have inspired scientists to study the underlying physics and retrace the origin of the mysterious pulses. In recent years, an increasing number of FRBs have been detected thanks to the improvement of detection techniques and the operation of new telescopes, such as the Canadian Hydrogen Intensity Mapping Experiment (CHIME, Collaboration et al. 2018) and the Five-hundred-meter Aperture Spherical Telescope (FAST, Nan et al. 2011), which gives us a new chance to deep investigate the Universe.

FRBs are very luminous and most of them have large dispersion measure (DM), indicating extragalactic or even cosmological origin (Lorimer et al. 2007; Thornton et al. 2013; Petroff et al. 2015, 2016). The direct measurement of redshift of FRB 150418 confirmed this hypothesis (Keane et al. 2016). Therefore, FRBs can be used to probe cosmological parameters such as the dark matter (Muñoz et al. 2016), the baryon mass density (Walters et al. 2018; Macquart et al. 2020), the baryon mass fraction in intergalactic medium (IGM) (Li et al. 2019a, 2020), the Hubble parameter (Wu et al. 2020) and Hubble constant

\* Corresponding author: zou Rui@stu.cqu.edu.cn

(Li et al. 2018), the cosmic curvature (Li et al. 2018), the cosmic proper distance (Yu & Wang 2017) and the reionization history of hydrogen and helium (Pagano & Fronenberg 2021), etc. Besides, FRBs can also be used to test the fundamental physics, such as constraining the rest mass of photon (Wu et al. 2016; Bonetti et al. 2016), testing the Einstein’s equivalence principle (Wei et al. 2015; Tingay & Kaplan 2016), and constraining the Lorentz invariance violation (Wei & Wu 2021). All these applications can be achieved from the DM-redshift relation.

One problem that hinders the applications of FRBs in cosmology is the strong degeneracy between cosmological parameters and the baryon mass fraction in IGM ( $f_{\text{IGM}}$ ). Fukugita et al. (1998) estimated that the baryons in stars and their remnants only comprise about 17% of the total baryon based on numerous observations, while the remaining 83% baryons are in a diffuse state in IGM. This is the so-called “missing baryon” problem. Since then, many numerical simulations (Cen & Ostriker 1999, 2006; Ferrara & Pandolfi 2014) and observations (Muñoz & Loeb 2018; Fukugita & Peebles 2004; Shull et al. 2012; McQuinn 2014; Hill et al. 2016) have been done in hope that the missing baryon problem would be alleviated. For example, Ferrara & Pandolfi (2014) estimated that of  $f_{\text{IGM}} = 0.82$  at  $z \leq 0.4$  and  $f_{\text{IGM}} = 0.9$  at  $z \geq 1.5$ , showing moderate redshift-evolution. FRBs, as the most energetic radio transients in the Universe, are excellent tools to probe the baryons. Li et al. (2019a) proposed a cosmology-independent method to estimate  $f_{\text{IGM}}$  using FRBs. Using this method, Li et al. (2020) obtained  $f_{\text{IGM}} = 0.84_{-0.22}^{+0.16}$  from five well-localized FRBs, but no evidence of redshift-dependence was found. In a word, the  $f_{\text{IGM}}$  term is still not well constrained, especially its redshift evolution.

There are several difficulties in using FRBs as probes to study the cosmology. First, the available FRB sample is not large enough. Though hundreds of FRBs have been detected, only a tiny number of them are well-localized and have redshift measurements. Second, due to the large-scale density fluctuations, the DM contribution of IGM,  $\text{DM}_{\text{IGM}}$ , has large uncertainty. The true value of  $\text{DM}_{\text{IGM}}$  may significantly deviate from the expectation (Macquart et al. 2020). Finally, the DM contribution of host galaxy,  $\text{DM}_{\text{host}}$ , is poorly known, which may be affected by many factors such as the galaxy type, the mass of host galaxy, the inclination angle of host galaxy, the star-formation rate (SFR), etc. Hence, to model  $\text{DM}_{\text{host}}$  is not an easy task. Some papers in the literature treat this term as a constant, or model it as SFR-dependent (Ioka 2003; Deng & Zhang 2014; Li et al. 2019a). However, the actual value of  $\text{DM}_{\text{host}}$  can vary significantly from burst to burst. Numerical simulations show that  $\text{DM}_{\text{host}}$  follow a certain probability distribution (Macquart et al. 2020; Zhang et al. 2020). Thus, properly dealing with  $\text{DM}_{\text{host}}$  is important when using FRBs to constrain cosmological parameters.

In this paper, we investigate the baryon mass fraction in IGM, especially its redshift evolution using well-localized FRBs. The probability distributions of  $\text{DM}_{\text{IGM}}$  and  $\text{DM}_{\text{host}}$  are properly taken into consideration. The Bayesian inference method is applied to constrain the free parameters. The rest parts of this paper are arranged as follows: In Section 2, we introduce a Bayesian framework to constrain the baryon mass fraction in IGM using FRBs. The observational data and the constraining results are given in Section 3. In Section 4, we perform Monte Carlo simulations to check the validity of our method. Finally, discussion and conclusions are given in Section 5.

## 2 METHODOLOGY

The propagation of FRBs can be easily influenced by the intervening medium between the host galaxy and the observer on earth. Most importantly, the interaction of radio waves with cold plasma leads to the delay of arriving time, i.e., the pulse with higher frequency arrives earlier than the lower one. The time delay caused by the plasma effect is proportional to a quantity named dispersion measure (DM), which can be expressed as the integral of the electron number density along the travelling path,  $\text{DM}_{\text{FRB}} = \int n_e dl / (1 + z)$ . Physically, the total DM of an FRB can be decomposed into four primary components (Gao et al. 2014; Deng & Zhang 2014; Macquart et al. 2020),

$$\text{DM}_{\text{FRB}}(z) = \text{DM}_{\text{MW,ISM}} + \text{DM}_{\text{MW,halo}} + \text{DM}_{\text{IGM}}(z) + \frac{\text{DM}_{\text{host}}}{1 + z}, \quad (1)$$

where  $\text{DM}_{\text{MW,ISM}}$  is the contribution from the Galactic interstellar medium (ISM),  $\text{DM}_{\text{MW,halo}}$  is the contribution from the Galactic halo,  $\text{DM}_{\text{host}}$  is the contribution from host galaxy in the source frame, which is weighted by  $(1 + z)^{-1}$  if converted to the observer frame, and  $\text{DM}_{\text{IGM}}$  is the contribution from IGM.

The  $\text{DM}_{\text{MW,ISM}}$  term can be estimated from the Galactic electron density models, such as the NE2001 model (Cordes & Lazio 2002) and the YMW16 model (Yao et al. 2017). These two models give consistent results at high Galactic latitude, but it is shown that the YMW16 model may overestimate  $\text{DM}_{\text{MW,ISM}}$  at low Galactic latitude (Koch Ocker et al. 2021). Therefore, we apply the NE2001 model to calculate  $\text{DM}_{\text{MW,ISM}}$ . We still have poor knowledge on the exact value of the  $\text{DM}_{\text{MW,halo}}$ . Prochaska & Zheng (2019) estimated that it is in the range of  $50 - 100 \text{ pc cm}^{-3}$ . Therefore, we follow Macquart et al. (2020) and conservatively assume  $\text{DM}_{\text{MW,halo}} = 50 \text{ pc cm}^{-3}$ . The value of  $\text{DM}_{\text{host}}$  may vary significantly in different sources, which will become less important at high redshift because of the  $(1 + z)^{-1}$  factor suppression and the domination of the  $\text{DM}_{\text{IGM}}$  term. But at low-redshift this term can’t be ignored. The  $\text{DM}_{\text{IGM}}$  term is strongly redshift-dependent, which contains the information of cosmological parameters. The probability distributions of  $\text{DM}_{\text{host}}$  and  $\text{DM}_{\text{IGM}}$  are discussed below.

Based on the standard  $\Lambda$ CDM model, the mean value of  $\text{DM}_{\text{IGM}}$  at redshift  $z$  can be written as (Deng & Zhang 2014;

Zhang et al. 2021a)

$$\langle \text{DM}_{\text{IGM}}(z) \rangle = \frac{3cH_0\Omega_b f_{\text{IGM}} f_e}{8\pi G m_p} \int_0^z \frac{1+z}{\sqrt{\Omega_m(1+z)^3 + \Omega_\Lambda}} dz, \quad (2)$$

where  $H_0$  is the Hubble constant,  $\Omega_b$  is the cosmic baryon mass density,  $\Omega_m$  and  $\Omega_\Lambda$  are the matter density and vacuum energy density of the Universe, respectively. The three constants  $c$ ,  $G$  and  $m_p$  are the speed of light, the Newtonian gravitational constant and the mass of proton, respectively.  $f_e = Y_{\text{H}} X_{e,\text{H}}(z) + \frac{1}{2} Y_{\text{He}} X_{e,\text{He}}(z)$  denotes the extent of ionization progress of hydrogen and helium, in which  $Y_{\text{H}} = 0.75$  and  $Y_{\text{He}} = 0.25$  are the mass fractions of hydrogen and helium,  $X_{e,\text{H}}$  and  $X_{e,\text{He}}$  are their ionization fractions, respectively. Considering both hydrogen and helium are fully ionized at  $z < 3$  (Meiksin 2009; Becker et al. 2011), we take  $X_{e,\text{H}} = X_{e,\text{He}} = 1$ .  $f_{\text{IGM}}$  is the fraction of baryon mass in IGM, which may slowly increase with redshift (Ferrara & Pandolfi 2014), but the accurate form is still unclear. In this paper, we follow Li et al. (2019a) and phenomenological parameterize it as a mildly evolving function of redshift,

$$f_{\text{IGM}}(z) = f_{\text{IGM},0} \left( 1 + \frac{\alpha z}{1+z} \right), \quad (3)$$

where  $f_{\text{IGM},0}$  is the baryon mass fraction in IGM at  $z = 0$ , and  $\alpha$  is the evolving parameter that are expected to prefer a positive value (Li et al. 2019a; McQuinn 2014). We work in the standard  $\Lambda$ CDM model with the Planck 2018 parameters, i.e.,  $H_0 = 67.4 \text{ km s}^{-1} \text{ Mpc}^{-1}$ ,  $\Omega_m = 0.315$ ,  $\Omega_\Lambda = 0.685$  and  $\Omega_b = 0.0493$  (Aghanim et al. 2020).

Although the mean value of  $\text{DM}_{\text{IGM}}$  is given in equation (2), the actual value of this term will vary around the mean due to the large-scale fluctuations. The probability density function of  $\text{DM}_{\text{IGM}}$  can be derived from theoretical analyses of the IGM and galaxy haloes (McQuinn 2014; Prochaska & Zheng 2019), which can be fitted using the function (Macquart et al. 2020; Zhang et al. 2021b)

$$p_{\text{IGM}}(\Delta) = A \Delta^{-\beta} \exp \left[ -\frac{(\Delta^{-\alpha} - C_0)^2}{2\alpha^2 \sigma_{\text{IGM}}^2} \right], \quad \Delta > 0, \quad (4)$$

where  $\Delta \equiv \text{DM}_{\text{IGM}} / \langle \text{DM}_{\text{IGM}} \rangle$ , and  $\sigma_{\text{IGM}} = F z^{-0.5}$  represents the effective standard deviation, with  $F$  being the baryon feedback coefficient.  $\alpha$  and  $\beta$  are two parameters related to the inner density profile of gas in haloes, which are chosen to be  $\alpha = \beta = 3$  (Macquart et al. 2020).  $A$  is the normalization constant, and  $C_0$  is calculated to make sure that the mean of the distribution is unity.

The distribution of  $\text{DM}_{\text{host}}$  has limited theoretical motivation because of the absence of information about the local environment of FRB sources. It may range from several ten to several hundred  $\text{pc cm}^{-3}$ . For example, Xu et al. (2022) estimated the  $\text{DM}_{\text{host}}$  of FRB20201124A to be in the range of  $10 \sim 310 \text{ pc cm}^{-3}$ , while Niu et al. (2022) estimated that of FRB20190520B to be as large as  $900 \text{ pc cm}^{-3}$ . To account for the possible existence of large  $\text{DM}_{\text{host}}$  value, we assume that it follows the log-normal distribution (Macquart et al. 2020; Zhang et al. 2020),

$$p_{\text{host}}(\text{DM}_{\text{host}} | \mu, \sigma_{\text{host}}) = \frac{1}{\sqrt{2\pi} \text{DM}_{\text{host}} \sigma_{\text{host}}} \exp \left[ -\frac{(\ln \text{DM}_{\text{host}} - \mu)^2}{2\sigma_{\text{host}}^2} \right], \quad (5)$$

where  $\mu$  and  $\sigma_{\text{host}}$  denote the mean and standard deviation of  $\ln \text{DM}_{\text{host}}$ , respectively. Generally,  $\mu$  and  $\sigma_{\text{host}}$  should be redshift dependent, but for non-repeating bursts they do not vary significantly with redshift (Zhang et al. 2020). For simplicity, we follow Macquart et al. (2020) and treat the two parameters as constants.

Since the DM contributions from the Milky Way (including  $\text{DM}_{\text{MW,ISM}}$  and  $\text{DM}_{\text{MW,halo}}$ ) can be estimated directly, we can subtract them from the total DM. For simplicity, we define the extragalactic DM as

$$\text{DM}_{\text{E}} \equiv \text{DM}_{\text{FRB}} - \text{DM}_{\text{MW,ISM}} - \text{DM}_{\text{MW,halo}} = \text{DM}_{\text{IGM}} + \frac{\text{DM}_{\text{host}}}{1+z}. \quad (6)$$

Based on the probability distributions of  $\text{DM}_{\text{IGM}}$  and  $\text{DM}_{\text{host}}$ , the probability distribution of  $\text{DM}_{\text{E}}$  can be calculated as

$$p_{\text{E}}(\text{DM}_{\text{E}} | z) = \int_0^{(1+z)\text{DM}_{\text{E}}} p_{\text{host}}(\text{DM}_{\text{host}} | \mu, \sigma_{\text{host}}) p_{\text{IGM}}(\text{DM}_{\text{E}} - \frac{\text{DM}_{\text{host}}}{1+z} | F, f_{\text{IGM},0}, \alpha) d\text{DM}_{\text{host}}. \quad (7)$$

Then the joint likelihood function of a sample of FRBs can be written as

$$\mathcal{L} = \prod_{i=1}^N p_{\text{E}}(\text{DM}_{\text{E},i} | z_i), \quad (8)$$

where  $N$  is the total number of FRBs. According to the Bayesian theorem, the posterior probability density function of the free parameters can be written as

$$P(F, f_{\text{IGM},0}, \alpha, \mu, \sigma_{\text{host}} | \text{FRBs}) \propto \mathcal{L}(\text{FRBs} | F, f_{\text{IGM},0}, \alpha, \mu, \sigma_{\text{host}}) P_0(F, f_{\text{IGM},0}, \alpha, \mu, \sigma_{\text{host}}), \quad (9)$$

where  $P_0$  is the prior of the free parameters. There are five free parameters in total: three parameters related to  $\text{DM}_{\text{IGM}}$  ( $F$ ,  $f_{\text{IGM},0}$  and  $\alpha$ ), and two parameters related to  $\text{DM}_{\text{host}}$  ( $\mu$  and  $\sigma_{\text{host}}$ ), which will be constrained simultaneously using well-localized FRBs in the next section.

†

**Table 1.** The catalog of 18 well-localized FRBs.  $DM_{MW,ISM}$  is calculated using NE2001 model, and  $DM_E$  is calculated with equation (6) by assuming  $DM_{MW,halo} = 50 \text{ pc cm}^{-3}$ .

FRBs	RA [ $^{\circ}$ ]	Dec [ $^{\circ}$ ]	$DM_{FRB}$ [ $\text{pc cm}^{-3}$ ]	$DM_{MW,ISM}$ [ $\text{pc cm}^{-3}$ ]	$DM_E$ [ $\text{pc cm}^{-3}$ ]	$z_{sp}$	repeat?	reference
20121102A	82.99	33.15	557.00	157.60	349.40	0.1927	Yes	Chatterjee et al. (2017)
20171020A	22.15	-19.40	114.10	38.00	26.10	0.0087	No	Li et al. (2019b)
20180301A	93.23	4.67	536.00	136.53	349.47	0.3305	Yes	Bhandari et al. (2022)
20180916B	29.50	65.72	348.80	168.73	130.07	0.0337	Yes	Marcote et al. (2020)
20180924B	326.11	-40.90	362.16	41.45	270.71	0.3214	No	Bannister et al. (2019)
20181030A	158.60	73.76	103.50	40.16	13.34	0.0039	Yes	Bhardwaj et al. (2021b)
20181112A	327.35	-52.97	589.00	41.98	497.02	0.4755	No	Prochaska et al. (2019)
20190102C	322.42	-79.48	364.55	56.22	258.33	0.2913	No	Macquart et al. (2020)
20190523A	207.06	72.47	760.80	36.74	674.06	0.6600	No	Ravi et al. (2019)
20190608B	334.02	-7.90	340.05	37.81	252.24	0.1178	No	Macquart et al. (2020)
20190611B	320.74	-79.40	332.63	56.60	226.03	0.3778	No	Macquart et al. (2020)
20190711A	329.42	-80.36	592.60	55.37	487.23	0.5217	Yes	Macquart et al. (2020)
20190714A	183.98	-13.02	504.13	38.00	416.13	0.2365	No	Heintz et al. (2020)
20191001A	323.35	-54.75	507.90	44.22	413.68	0.2340	No	Heintz et al. (2020)
20191228A	344.43	-29.59	297.50	33.75	213.75	0.2432	No	Bhandari et al. (2022)
20200430A	229.71	12.38	380.25	27.35	302.90	0.1608	No	Bhandari et al. (2022)
20200906A	53.50	-14.08	577.80	36.19	491.61	0.3688	No	Bhandari et al. (2022)
20201124A	77.01	26.06	413.52	126.49	237.03	0.0979	Yes	Fong et al. (2021)

**Table 2.** The best-fitting parameters ( $F$ ,  $f_{IGM,0}$ ,  $\alpha$ ,  $\sigma_{\text{host}}$ ,  $\exp(\mu)$ ) constrained from 18 well-localized FRBs. The uncertainties are given at  $1\sigma$  confidence level.

$F$	$f_{IGM,0}$	$\alpha$	$\sigma_{\text{host}}$	$\exp(\mu)/\text{pc cm}^{-3}$
$0.42^{+0.06}_{-0.10}$	$0.92^{+0.06}_{-0.12}$	$0.49^{+0.59}_{-0.47}$	$1.13^{+0.33}_{-0.24}$	$72.49^{+33.31}_{-25.62}$
$0.42^{+0.06}_{-0.10}$	0.84(fixed)	$0.77^{+0.40}_{-0.44}$	$1.18^{+0.34}_{-0.25}$	$74.63^{+32.05}_{-26.13}$
0.2(fixed)	0.84(fixed)	$0.11^{+0.24}_{-0.27}$	$1.14^{+0.32}_{-0.23}$	$87.44^{+34.86}_{-29.16}$

### 3 DATA AND RESULTS

Till now, there are 21 well-localized extragalactic FRBs that have accurate identification of host galaxy and direct measurement of redshifts<sup>1</sup>. Among them, FRB20200120E, FRB20190614D and FRB20190520B are ingored. The source of FRB20200120E is near our Galaxy, and the peculiar velocity dominates over the Hubble flow, so it has a negative spectroscopic redshift  $z = -0.001$  (Bhardwaj et al. 2021a; Kirsten et al. 2022). FRB20190614D doesn't have a direct measurement of spectroscopic redshift, but have a photometric redshift  $z \approx 0.6$  (Law et al. 2020). The  $DM_{\text{host}}$  of FRB20190520B is estimated to be as large as  $900 \text{ pc cm}^{-3}$  (Niu et al. 2022), which is much larger than the normal FRBs, so this FRB is also excluded in our sample. The remaining 18 FRBs have well measured spectroscopic redshifts, and their main properties are listed in Table 1, which will be used to constrain cosmological parameters.

In the ideal case, we hope that all the five parameters ( $F$ ,  $f_{IGM,0}$ ,  $\alpha$ ,  $\sigma_{\text{host}}$ ,  $\exp(\mu)$ ) can be simultaneously constrained well. In practice, we use  $\exp(\mu)$  instead of  $\mu$  as a free parameter, because  $\exp(\mu)$  directly represents the median value of  $DM_{\text{host}}$ . The posterior probability density functions of the free parameters are calculated with the publicly available Python package code `emcee` (Foreman-Mackey et al. 2013). Flat priors are used for all the five parameters:  $F \in U(0.01, 0.5)$ ,  $f_{IGM,0} \in U(0, 1)$ ,  $\alpha \in U(-2, 2)$ ,  $\sigma_{\text{host}} \in U(0.2, 2)$ , and  $\exp(\mu) \in U(20, 200) \text{ pc cm}^{-3}$ . The 2D marginalized posterior distributions and the  $1-3\sigma$  confidence contours of the five parameters are plotted in the left panel of Figure 1, together with the best-fitting parameters listed in Table 2. One can see that although  $\sigma_{\text{host}}$  and  $\exp(\mu)$  are tightly constrained, the constraints on  $F$ ,  $f_{IGM,0}$  and  $\alpha$  are not strict. One possible factor is that the FRB sample is not large enough to simultaneously constrain a model with too many free parameters. To reduce the freedom, we try to fix one or two parameters that can be constrained from other observations, to see if the FRB sample can strictly constrain the remaining parameters or not.

The fraction of baryon mass in IGM in the local Universe,  $f_{IGM,0}$ , has been constrained by various observations. For instance, Fukugita et al. (1998) obtained  $f_{IGM,0} \approx 0.83$  from directly observing the budget of baryons in different states.

<sup>1</sup> There are 19 well-localized FRBs compiled in the FRB Host Database, <http://frbhosts.org/>. Two other FRBs, FRB20171020A (Li et al. 2019b) and FRB20190520B (Niu et al. 2022), are not included in the database.

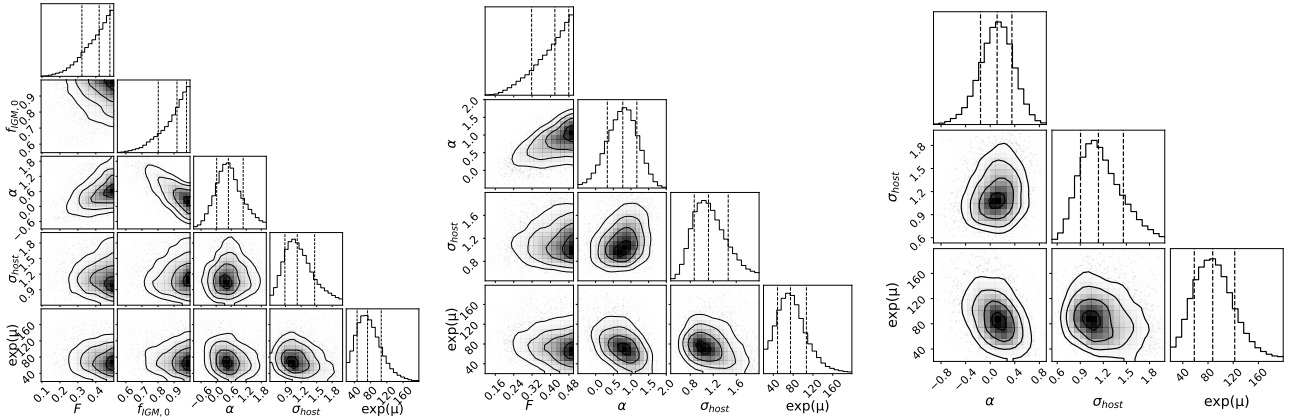


**Figure 1.** The contour plots constrained from 18 well-localized FRBs. The dashed lines from left to right in each subfigure represent the 16%, 50% and 84% quantiles of the distribution, respectively. Left panel: constraints on five parameters; Middle panel: constraints on four parameters with  $f_{\text{IGM},0} = 0.84$  fixed; Right panel: constraints on three parameters with  $f_{\text{IGM},0} = 0.84$  and  $F = 0.2$  fixed.

Ferrara & Pandolfi (2014) investigated the reionization history of IGM, and estimated that  $f_{\text{IGM}} \approx 0.82$  at  $z \lesssim 0.4$ , which mildly increases to  $f_{\text{IGM}} \approx 0.9$  at  $z \gtrsim 1.5$ . Based on five well-localized FRBs, Li et al. (2020) obtained  $f_{\text{IGM},0} = 0.84^{+0.16}_{-0.22}$ , but no strong evidence for redshift evolution was found. All these results are consistent with each other within uncertainty. Therefore, to reduce the freedom, we first fix  $f_{\text{IGM},0} = 0.84$  and constrain the remaining four parameters. The confidence contours and the marginalized probability distributions of the remaining parameters are plotted in the middle panel of Figure 1, and the best-fitting parameters are summarized in Table 2. We see that the uncertainty on  $\alpha$  is slightly reduced, but the constraints on the other parameters hardly change. Especially, the parameter  $F$  is still not well constrained.

Actually, the parameter  $F$  prefers a value around  $F = 0.2$  or even smaller at  $z \leq 1$  (Jaroszynski 2019; Kumar & Linder 2019). However, the constraint from our FRB sample prefers a much larger value,  $F \gtrsim 0.4$ , which may cause bias on the other parameters. Therefore, we additionally fix  $F = 0.2$ , and keep the other three parameters ( $\alpha$ ,  $\sigma_{\text{host}}$ ,  $\exp(\mu)$ ) free. The contour plots are demonstrated in the right panel of Figure 1, and the best-fitting parameters are summarized in Table 2. As can be seen, fixing  $F$  further reduces the uncertainty on  $\alpha$ , but does not strongly affect the uncertainties on  $\sigma_{\text{host}}$  and  $\exp(\mu)$ . In addition, fixing  $F$  strongly affects the central values of  $\alpha$  and  $\exp(\mu)$ , but does not significantly affect the central value of  $\sigma_{\text{host}}$ . The result of  $\alpha = 0.11^{+0.24}_{-0.27}$  is consistent with the truth that  $f_{\text{IGM}}$  may slowly increase with redshift. But due to the large uncertainty, it is still consistent with no redshift evolution. A much larger FRB sample in a wider redshift range may help us to further reduce the uncertainty. To check this, we perform Monte Carlo simulations, which will be discussed in detail in the next section.

#### 4 MONTE CARLO SIMULATIONS

With the progress of detection technique, more and more FRBs are expected to be discovered in the future, and a fraction of them can be well-localized. In addition, FRBs at high redshift may be detectable as the improvement of sensitivity of radio telescopes such as the FAST (Nan et al. 2011). Therefore, it is interesting to investigate the constraining ability on cosmological parameters if a large sample of FRBs in a wide redshift range are available. To this end, we perform Monte Carlo simulations to test the efficiency of our method.

The intrinsic redshift distribution of FRBs is still unclear due to the small well-localized sample. Several possibilities have been discussed in some papers. For example, Yu & Wang (2017) assumed that FRBs may have a similar redshift distribution to gamma-ray bursts, Li et al. (2019a) assumed that FRBs have a constant comoving number density but with a Gaussian cutoff, Zhang et al. (2021a) argued that the redshift distribution of FRBs is expected to be related with SFR, or influenced by the compact star merger but with an additional time delay. In this paper, we adopt the SFR-related model, in which the probability density function takes the form (Zhang et al. 2021a)

$$P(z) \propto \frac{4\pi D_c^2(z) \text{SFR}(z)}{(1+z)H(z)}, \quad (10)$$

where  $D_c(z) = \int_0^z \frac{cdz}{H(z)}$  represents the comoving distance, with  $c$  the speed of light and  $H(z) = H_0 \sqrt{\Omega_m(1+z)^3 + \Omega_\Lambda}$  the

**Table 3.** The best-fitting parameters ( $F$ ,  $\alpha$ ,  $\sigma_{\text{host}}$ ,  $\exp(\mu)$ ) constrained from  $N = 100, 200$  and  $300$  mock FRBs. The fiducial values are  $F = 0.2$ ,  $\alpha = 0$  (left panel) and  $\alpha = 0.2$  (right panel),  $\sigma_{\text{host}} = 1.0$  and  $\exp(\mu) = 100 \text{ pc cm}^{-3}$ . The uncertainties are given at  $1\sigma$  confidence level.

$N$	$F$	$\alpha$	$\sigma_{\text{host}}$	$\exp(\mu)/\text{pc cm}^{-3}$	$N$	$F$	$\alpha$	$\sigma_{\text{host}}$	$\exp(\mu)/\text{pc cm}^{-3}$
100	$0.17^{+0.04}_{-0.03}$	$0.00^{+0.05}_{-0.04}$	$0.55^{+0.31}_{-0.23}$	$61.45^{+34.61}_{-24.95}$	100	$0.18^{+0.05}_{-0.03}$	$0.21^{+0.07}_{-0.04}$	$0.76^{+0.26}_{-0.26}$	$79.21^{+39.03}_{-29.77}$
200	$0.19^{+0.04}_{-0.02}$	$0.02^{+0.04}_{-0.03}$	$0.52^{+0.29}_{-0.22}$	$90.25^{+36.09}_{-32.25}$	200	$0.18^{+0.03}_{-0.02}$	$0.23^{+0.04}_{-0.03}$	$0.65^{+0.25}_{-0.28}$	$61.76^{+29.61}_{-22.99}$
300	$0.17^{+0.02}_{-0.01}$	$0.02^{+0.03}_{-0.02}$	$0.74^{+0.20}_{-0.27}$	$56.84^{+21.88}_{-17.19}$	300	$0.19^{+0.03}_{-0.02}$	$0.22^{+0.04}_{-0.03}$	$0.60^{+0.28}_{-0.26}$	$87.58^{+30.96}_{-26.59}$

**Table 4.** The best-fitting parameters ( $\alpha$ ,  $\sigma_{\text{host}}$ ,  $\exp(\mu)$ ) constrained from  $N = 100, 200$  and  $300$  mock FRBs. The fiducial values are  $F = 0.2$ ,  $\alpha = 0$  (left panel) and  $\alpha = 0.2$  (right panel),  $\sigma_{\text{host}} = 1.0$  and  $\exp(\mu) = 100 \text{ pc cm}^{-3}$ . The uncertainties are given at  $1\sigma$  level.

$N$	$\alpha$	$\sigma_{\text{host}}$	$\exp(\mu)/\text{pc cm}^{-3}$	$N$	$\alpha$	$\sigma_{\text{host}}$	$\exp(\mu)/\text{pc cm}^{-3}$
100	$0.02^{+0.02}_{-0.02}$	$0.72^{+0.29}_{-0.28}$	$99.49^{+39.89}_{-35.38}$	100	$0.22^{+0.03}_{-0.03}$	$0.86^{+0.30}_{-0.34}$	$76.87^{+35.41}_{-27.48}$
200	$0.01^{+0.02}_{-0.02}$	$0.94^{+0.22}_{-0.29}$	$82.90^{+27.14}_{-21.99}$	200	$0.21^{+0.02}_{-0.02}$	$0.94^{+0.19}_{-0.21}$	$85.07^{+27.11}_{-23.51}$
300	$0.01^{+0.01}_{-0.01}$	$1.11^{+0.17}_{-0.18}$	$82.24^{+21.55}_{-18.77}$	300	$0.21^{+0.02}_{-0.02}$	$0.97^{+0.15}_{-0.19}$	$88.76^{+24.46}_{-20.78}$

Hubble expansion rate, and the SFR takes the form (Yuksel et al. 2008)

$$\text{SFR}(z) = 0.02 \left[ (1+z)^{a\eta} + \left(\frac{1+z}{B}\right)^{b\eta} + \left(\frac{1+z}{C}\right)^{c\eta} \right]^{1/\eta}, \quad (11)$$

where  $a = 3.4$ ,  $b = -0.3$ ,  $c = -3.5$ ,  $B = 5000$ ,  $C = 9$  and  $\eta = -10$ .

We simulate a set of mock FRB samples, and use them to constrain the parameters ( $F$ ,  $\alpha$ ,  $\sigma_{\text{host}}$ ,  $\exp(\mu)$ ). The simulations are performed based on the standard  $\Lambda$ CDM model with Planck 2018 parameters (Aghanim et al. 2020). The other fiducial parameters are  $F = 0.2$ ,  $f_{\text{IGM},0} = 0.84$ ,  $\alpha = 0$  or  $0.2$ ,  $\sigma_{\text{host}} = 1.0$  and  $\exp(\mu) = 100 \text{ pc cm}^{-3}$ . The main procedures of the simulations are described below.

- (1) Randomly draw a certain number of redshifts from equation (10). We set  $z_{\text{max}} = 3$ .
- (2) Calculate  $\langle \text{DM}_{\text{IGM}}(z) \rangle$  according to equation (2).
- (3) Randomly draw the same number of  $\Delta$  from equation (4).
- (4) Calculate  $\text{DM}_{\text{IGM}} = \Delta \times \langle \text{DM}_{\text{IGM}}(z) \rangle$ .
- (5) Randomly draw the same number of  $\text{DM}_{\text{host}}$  from equation (5).
- (6) Calculate  $\text{DM}_{\text{E}}$  according to the second equality of equation (6).
- (7) Finally, we obtain a sample of mock FRBs ( $z_i, \text{DM}_{\text{E}i}$ ),  $i = 1, 2, \dots, N$ .

We replace the true FRB samples with the mock samples, and use them to constrain the parameters as described above. First, we use the mock FRB samples to test the efficiency of our four-parameter model (with  $f_{\text{IGM},0} = 0.84$  fixed). The corresponding contour plots with  $N = 100, 200$  and  $300$  FRBs are shown in Figure 2. We consider two different fiducial values of  $\alpha$ , i.e.  $\alpha = 0$  (top three panels) and  $\alpha = 0.2$  (bottom three panels). We summarize the best-fitting parameters and their  $1\sigma$  uncertainties in Table 3. With the mock FRB samples, all the four parameters can be well constrained. However, we note that although  $F$  and  $\alpha$  correctly recover their fiducial values within  $1\sigma$  uncertainty in most cases,  $\sigma_{\text{host}}$  and  $\exp(\mu)$  are usually biased. The best-fitting values of  $\sigma_{\text{host}}$  and  $\exp(\mu)$  are usually smaller than their fiducial values. Two reasons may lead to this situation. First,  $\sigma_{\text{host}}$  and  $\exp(\mu)$  are two parameters related to  $\text{DM}_{\text{host}}$ , which gets less weight in  $\text{DM}_{\text{E}}$  at higher redshift. This results in less sensitivity on  $\sigma_{\text{host}}$  and  $\exp(\mu)$  in the Bayesian inference model. Second, the parameters are correlated. A biased estimation on one parameter may cause bias on the other parameters. We hope that fix one parameter (for example  $F$ ) may alleviate the bias.

To check this, we additionally fix  $F = 0.2$ , and use the same mock samples to constrain three parameters ( $\alpha$ ,  $\sigma_{\text{host}}$ ,  $\exp(\mu)$ ) in the identical manner to the previous four-parameter model. Through the combined contour plots (Figure 3) and the best-fitting results (Table 4), one can see that all the parameters correctly recover the fiducial values within  $1\sigma$  uncertainty. Compared with the true FRB samples, the parameter  $\alpha$  is more tightly constrained, thanks to the enlargement of FRB sample and the extension of redshift range. In addition, the uncertainties on  $\sigma_{\text{host}}$  and  $\exp(\mu)$  are reduced gradually with the increase of FRB number.

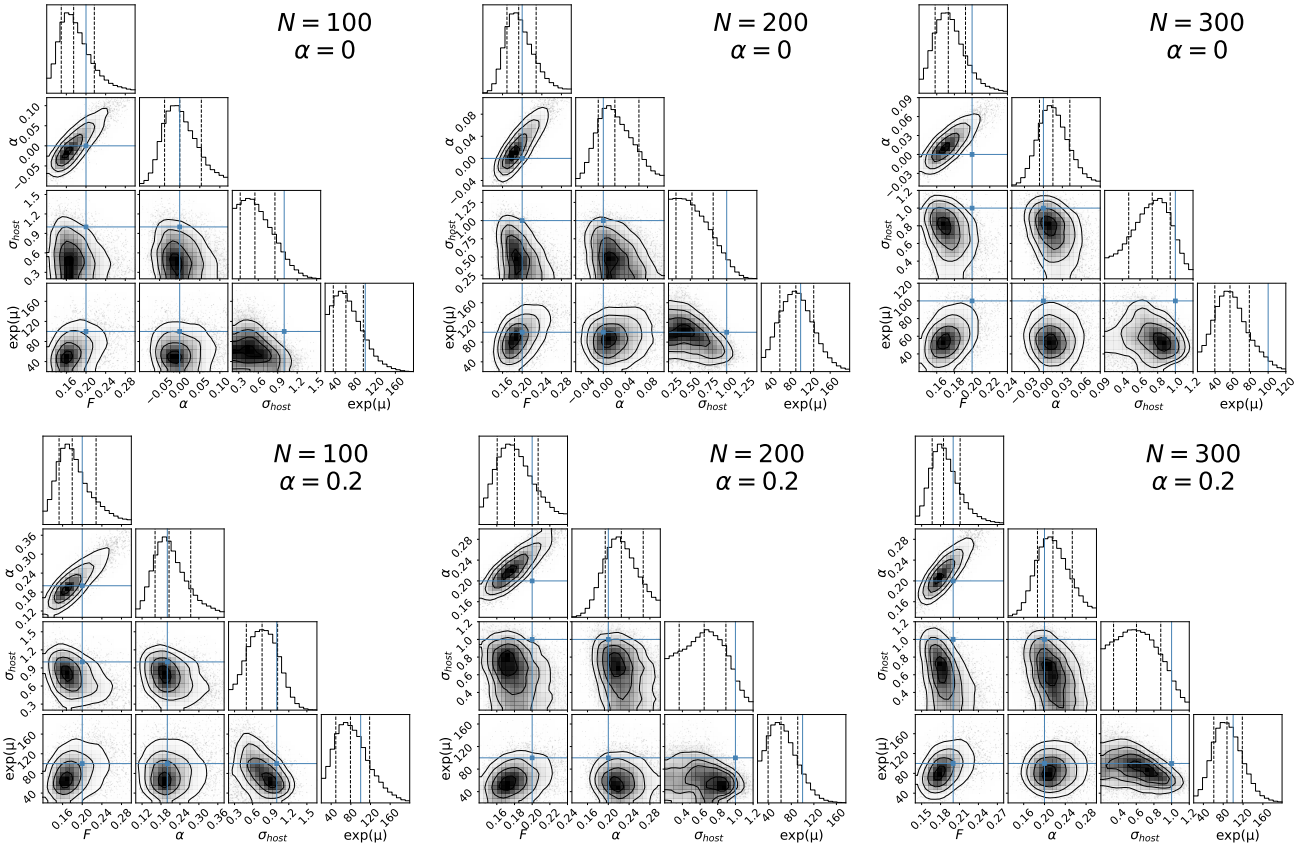


**Figure 2.** Constraints on four parameters ( $F$ ,  $\alpha$ ,  $\sigma_{\text{host}}$ ,  $\exp(\mu)$ ) by using  $N = 100, 200, 300$  (from left to right) mock FRBs, respectively. The fiducial values are  $F = 0.2$ ,  $\alpha = 0$  (top) and  $\alpha = 0.2$  (bottom),  $\sigma_{\text{host}} = 1.0$  and  $\exp(\mu) = 100 \text{ pc cm}^{-3}$ , which are reflected by the solid, blue lines. The dashed lines from left to right represent the 16%, 50% and 84% quantiles of the distribution, respectively.

## 5 DISCUSSION AND CONCLUSIONS

In this paper, we investigate the baryon mass fraction in IGM using well-localized FRBs. Considering the probability distributions of  $\text{DM}_{\text{IGM}}$  and  $\text{DM}_{\text{host}}$ , we construct a five-parameter Bayesian inference model. The free parameters ( $F$ ,  $f_{\text{IGM},0}$ ,  $\alpha$ ,  $\sigma_{\text{host}}$ ,  $\exp(\mu)$ ) are constrained using 18 well-localized FRBs that have direct redshift measurement. Unfortunately, due to the small FRB sample, the five parameters can't be well constrained simultaneously. Especially, the best-fitting value of  $f_{\text{IGM},0}$  is somewhat larger than expected, and the constraint on  $\alpha$  is loose. Considering that the fraction of baryon mass in the local universe can be constrained from other independent observations, we fix the parameter  $f_{\text{IGM},0} = 0.84$  and free the remaining four parameters. The uncertainty on  $\alpha$  is slightly reduced in four-parameter fit, but the parameter  $F$  is still not well-constrained. If we further fix  $F = 0.2$ , the remaining three parameters can be tightly constrained, with the best-fitting results  $\alpha = 0.11^{+0.24}_{-0.27}$ ,  $\sigma_{\text{host}} = 1.14^{+0.32}_{-0.23}$  and  $\exp(\mu) = 87.44^{+34.86}_{-29.16} \text{ pc cm}^{-3}$ . The positive central value of  $\alpha$  is consistent with the possibility that  $f_{\text{IGM}}$  may slowly increase with redshift, but due to the large uncertainty it is still consistent with no redshift evolution. Therefore, the present FRB sample is not large enough to prove or falsify the redshift dependence of baryon mass fraction in IGM.

With the operation of ongoing and upcoming radio telescopes, the available FRB sample is expected to be significantly enlarged in the near future. At the same time, the detectable redshift range is expected to be highly extended up to  $z \approx 3$ . To this end, we perform Monte Carlo simulations to check the efficiency of our method. It is found that even if we enlarge the FRB sample to  $N = 300$ , the five parameters can't be tightly constrained simultaneously. Fixing  $f_{\text{IGM},0}$  helps to improve the constraints on  $\alpha$ , but the parameters  $F$  still can't be well constrained. In addition, the parameters  $\sigma_{\text{host}}$  and  $\exp(\mu)$  may be biased. Only if we simultaneously fix the two parameters  $f_{\text{IGM},0}$  and  $F$ , we can achieve an unbiased estimation on the remaining parameters. In this case, the parameter  $\alpha$  are tightly constrained, at the level of  $\sim 0.02$  with  $N = 100$ . Therefore, in order to test the redshift dependence of baryon mass fraction in IGM using FRBs, precise constraints on  $f_{\text{IGM},0}$  and  $F$  using other independent observations are necessary.

We note that there is correlation between parameters. For instance, in the case of fixed  $F$  and  $f_{\text{IGM},0}$ , a larger  $\alpha$  value means a larger contribution of  $\text{DM}_{\text{IGM}}$  thus a smaller contribution of  $\text{DM}_{\text{host}}$ , hence a smaller value of  $\exp(\mu)$ . Therefore,  $\alpha$

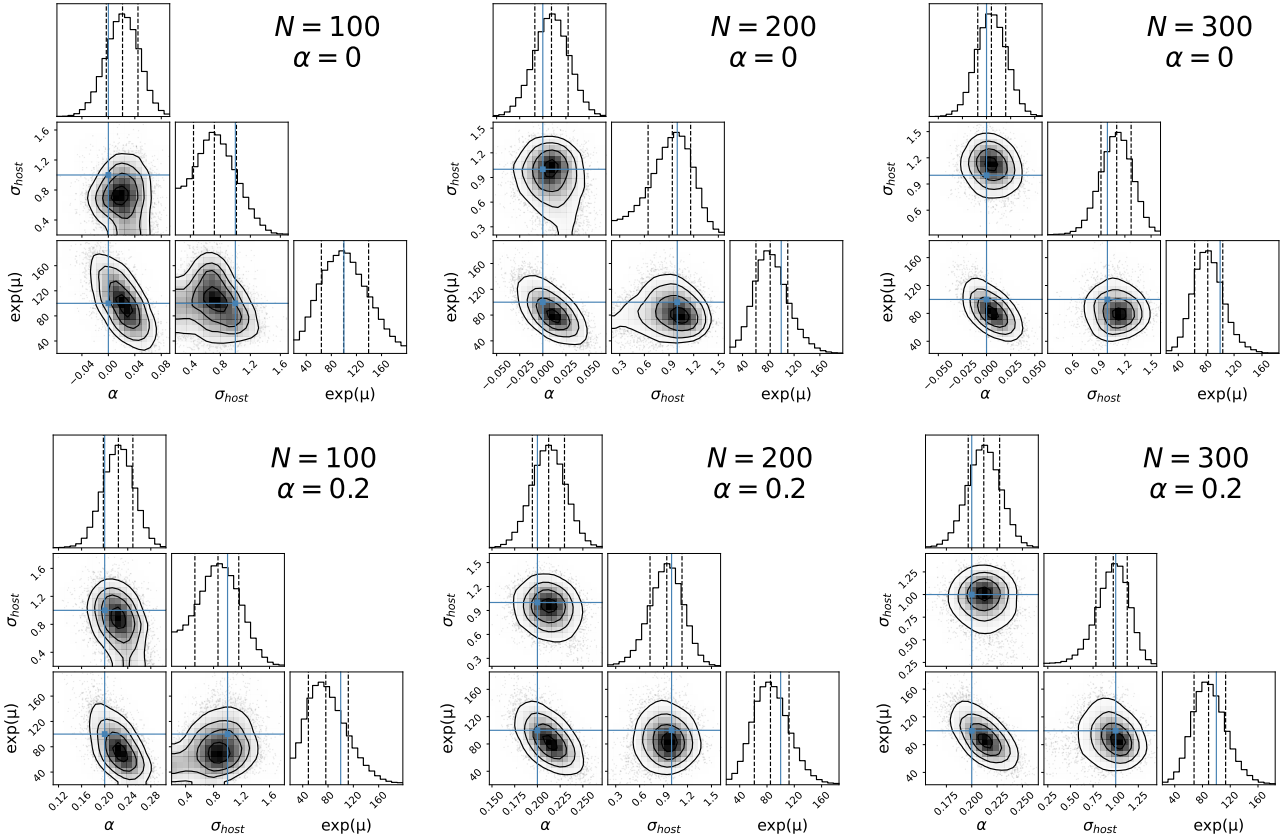


**Figure 3.** Constraints on three parameters ( $\alpha$ ,  $\sigma_{\text{host}}$ ,  $\text{exp}(\mu)$ ) by using  $N = 100, 200, 300$  (from left to right) mock FRBs, respectively. The fiducial values are  $F = 0.2$ ,  $\alpha = 0$  (top) and  $\alpha = 0.2$  (bottom),  $\sigma_{\text{host}} = 1.0$  and  $\text{exp}(\mu) = 100 \text{ pc cm}^{-3}$ , which are reflected by the solid, blue lines. The dashed lines from left to right represent the 16%, 50% and 84% quantiles of the distribution, respectively.

and  $\text{exp}(\mu)$  are negatively correlated. This can be seen clearly from the contour plot in the right panel of Figure 1 (and also Figure 3). For the fixed  $f_{\text{IGM},0}$ , a larger value of  $F$  means a larger variance of  $\text{DM}_{\text{IGM}}$ , hence the probability of  $\text{DM}_{\text{IGM}}$  being large is higher, which leads to a larger value of  $\alpha$ . Therefore,  $\alpha$  and  $F$  are positively correlated, see the contour plot in the middle panel of Figure 1 (this can be seen more clearly from Figure 2). From the left panel of Figure 1, we can also see that  $f_{\text{IGM},0}$  is negatively correlated with  $\alpha$ . This is a natural result, since for a fixed  $\text{DM}_{\text{IGM}}$  value, a larger  $f_{\text{IGM},0}$  value requires a smaller  $\alpha$  value. The parameter correlation explains why the five parameters can't be tightly constrained simultaneously, even if the data sample is enlarged.

## ACKNOWLEDGEMENTS

This work has been supported by the National Natural Science Fund of China (Grant Nos. 12275034, 11873001 and 12147102), and the Fundamental Research Funds for the Central Universities of China (Grants No. 2022CDJXY-002).

## DATA AVAILABILITY

The Host/FRB catalog is available at the FRB Host Database <http://frbhosts.org>.

## References

- Aghanim N., et al., 2020, *Astron. Astrophys.*, 641, A6  
 Amiri M., et al., 2021, *Astrophys. J. Supp.*, 257, 59  
 Andersen B. C., et al., 2020, *Nature*, 587, 54  
 Bannister K. W., et al., 2019, *Science*, 365, 565  
 Becker G. D., Bolton J. S., Haehnelt M. G., Sargent W. L. W., 2011, *Mon. Not. Roy. Astron. Soc.*, 410, 1096  
 Bhandari S., et al., 2022, *Astron. J.*, 163, 69



- Bhardwaj M., et al., 2021a, *Astrophys. J. Lett.*, 910, L18  
 Bhardwaj M., et al., 2021b, *Astrophys. J. Lett.*, 919, L24  
 Bochenek C. D., Ravi V., Belov K. V., Hallinan G., Kocz J., Kulkarni S. R., McKenna D. L., 2020, *Nature*, 587, 59  
 Bonetti L., Ellis J., Mavromatos N. E., Sakharov A. S., Sarkisyan-Grinbaum E. K. G., Spallicci A. D. A. M., 2016, *Phys. Lett. B*, 757, 548  
 Cen R., Ostriker J. P., 1999, *Astrophys. J.*, 514, 1  
 Cen R., Ostriker J. P., 2006, *Astrophys. J.*, 650, 560  
 Chatterjee S., et al., 2017, *Nature*, 541, 58  
 Collaboration T. C., et al., 2018, *The Astrophysical Journal*, 863, 48  
 Cordes J. M., Chatterjee S., 2019, *Ann. Rev. Astron. Astrophys.*, 57, 417  
 Cordes J. M., Lazio T. J. W., 2002, *arXiv: astro-ph/0207156*  
 Deng W., Zhang B., 2014, *Astrophys. J. Lett.*, 783, L35  
 Ferrara A., Pandolfi S., 2014, *Proc. Int. Sch. Phys. Fermi*, 186, 1  
 Fong W.-f., et al., 2021, *Astrophys. J. Lett.*, 919, L23  
 Foreman-Mackey D., Hogg D. W., Lang D., Goodman J., 2013, *Publ. Astron. Soc. Pac.*, 125, 306  
 Fukugita M., Peebles P. J. E., 2004, *Astrophys. J.*, 616, 643  
 Fukugita M., Hogan C. J., Peebles P. J. E., 1998, *Astrophys. J.*, 503, 518  
 Gao H., Li Z., Zhang B., 2014, *The Astrophysical Journal*, 788, 189  
 Heintz K. E., et al., 2020, *The Astrophysical Journal*, 903, 152  
 Hill J. C., Ferraro S., Battaglia N., Liu J., Spergel D. N., 2016, *Phys. Rev. Lett.*, 117, 051301  
 Ioka K., 2003, *Astrophys. J. Lett.*, 598, L79  
 Jaroszynski M., 2019, *Mon. Not. Roy. Astron. Soc.*, 484, 1637  
 Keane E. F., et al., 2016, *Nature*, 530, 453  
 Kirsten F., et al., 2022, *Nature*, 602, 585  
 Koch Ocker S., Cordes J. M., Chatterjee S., 2021, *Astrophys. J.*, 911, 102  
 Kumar P., Linder E. V., 2019, *Phys. Rev. D*, 100, 083533  
 Law C. J., et al., 2020, *Astrophys. J.*, 899, 161  
 Li Z.-X., Gao H., Ding X.-H., Wang G.-J., Zhang B., 2018, *Nature Commun.*, 9, 3833  
 Li Z., Gao H., Wei J.-J., Yang Y.-P., Zhang B., Zhu Z.-H., 2019a, *Astrophys. J.*, 876, 146  
 Li Y., Zhang B., Nagamine K., Shi J., 2019b, *Astrophys. J. Lett.*, 884, L26  
 Li Z., Gao H., Wei J.-J., Yang Y.-P., Zhang B., Zhu Z.-H., 2020, *Mon. Not. Roy. Astron. Soc.*, 496, L28  
 Lorimer D. R., Bailes M., McLaughlin M. A., Narkevic D. J., Crawford F., 2007, *Science*, 318, 777  
 Macquart J. P., et al., 2020, *Nature*, 581, 391  
 Marcote B., et al., 2017, *Astrophys. J. Lett.*, 834, L8  
 Marcote B., et al., 2020, *Nature*, 577, 190  
 McQuinn M., 2014, *Astrophys. J. Lett.*, 780, L33  
 Meiksin A. A., 2009, *Rev. Mod. Phys.*, 81, 1405  
 Muñoz J. B., Loeb A., 2018, *Phys. Rev. D*, 98, 103518  
 Muñoz J. B., Kovetz E. D., Dai L., Kamionkowski M., 2016, *Phys. Rev. Lett.*, 117, 091301  
 Nan R., et al., 2011, *Int. J. Mod. Phys. D*, 20, 989  
 Niu C. H., et al., 2022, *Nature*, 606, 873  
 Pagano M., Fronenberg H., 2021, *Mon. Not. Roy. Astron. Soc.*, 505, 2195  
 Petroff E., et al., 2015, *Mon. Not. Roy. Astron. Soc.*, 447, 246  
 Petroff E., et al., 2016, *Publ. Astron. Soc. Austral.*, 33, e045  
 Petroff E., Hessels J. W. T., Lorimer D. R., 2019, *Astron. Astrophys. Rev.*, 27, 4  
 Prochaska J. X., Zheng Y., 2019, *Monthly Notices of the Royal Astronomical Society*, 485, 648  
 Prochaska J. X., et al., 2019, *Science*, 366, 231  
 Ravi V., et al., 2019, *Nature*, 572, 352  
 Scholz P., et al., 2016, *Astrophys. J.*, 833, 177  
 Shull J. M., Smith B. D., Danforth C. W., 2012, *Astrophys. J.*, 759, 23  
 Spitler L. G., et al., 2016, *Nature*, 531, 202  
 Tendulkar S. P., et al., 2017, *Astrophys. J. Lett.*, 834, L7  
 Thornton D., et al., 2013, *Science*, 341, 53  
 Tingay S. J., Kaplan D. L., 2016, *Astrophys. J. Lett.*, 820, L31  
 Walters A., Weltman A., Gaensler B. M., Ma Y.-Z., Witzemann A., 2018, *Astrophys. J.*, 856, 65  
 Wei J.-J., Wu X.-F., 2021, *Front. Phys.*, 16, 44300  
 Wei J.-J., Gao H., Wu X.-F., Mészáros P., 2015, *Phys. Rev. Lett.*, 115, 261101  
 Wu X.-F., et al., 2016, *Astrophys. J. Lett.*, 822, L15  
 Wu Q., Yu H., Wang F. Y., 2020, *Astrophys. J.*, 895, 33  
 Xiao D., Wang F., Dai Z., 2021, *Sci. China Phys. Mech. Astron.*, 64, 249501  
 Xu H., et al., 2022, *Nature*, 609, 685  
 Yao J. M., Manchester R. N., Wang N., 2017, *The Astrophysical Journal*, 835, 29  
 Yu H., Wang F. Y., 2017, *Astron. Astrophys.*, 606, A3  
 Yuksel H., Kistler M. D., Beacom J. F., Hopkins A. M., 2008, *Astrophys. J. Lett.*, 683, L5  
 Zhang B., 2022, *arXiv: 2212.03972*  
 Zhang G. Q., Yu H., He J. H., Wang F. Y., 2020, *Astrophys. J.*, 900, 170  
 Zhang R. C., Zhang B., Li Y., Lorimer D. R., 2021a, *Mon. Not. Roy. Astron. Soc.*, 501, 157  
 Zhang Z. J., Yan K., Li C. M., Zhang G. Q., Wang F. Y., 2021b, *Astrophys. J.*, 906, 49